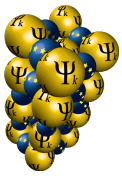

Ψ_k **Scientific Highlight Of The Month**

No. 141 **June 2018**

First principles calculation of spin related quantities for point defect qubit research

Viktor Ivády[1,2,*], Igor A. Abrikosov[1,3], and Adam Gali[2,4]

[1] *Department of Physics, Chemistry and Biology, Linköping University, SE-581 83 Linköping, Sweden*

[2] *Wigner Research Centre for Physics, Hungarian Academy of Sciences, PO Box 49, H-1525, Budapest, Hungary*

[3] *Materials Modeling and Development Laboratory, National University of Science and Technology 'MISIS', 119049 Moscow, Russia*

[4] *Department of Atomic Physics, Budapest University of Technology and Economics, Budafoki út 8., H-1111 Budapest, Hungary*

Abstract

Point defect research in semiconductors has gained remarkable new momentum due to the identification of special point defects that can implement qubits and single photon emitters with unique characteristics. Indeed, these implementations are among the few alternatives for quantum technologies that may operate even at room temperature, and therefore discoveries and characterization of novel point defects may highly facilitate future solid state quantum technologies. First principles calculations play an important role in point defect research since they provide a direct, extended insight into the formation of the defect states. In last decades, considerable efforts have been made to calculate spin dependent properties of point defects from first principles. The developed methods have already demonstrated their essential role in quantitative understanding of the physics and application of point defect qubits. Here, we review and discuss accuracy aspects of these novel *ab initio* methods and report on their most relevant applications for existing point defect qubits in semiconductors. We pay attention to the advantages and limitations of the methodological solutions and highlight additional developments that are expected in the near future. Moreover, we discuss the opportunity of a systematic search for potential point defect qubits as well as the possible development of predictive spin dynamic simulations facilitated by *ab initio* calculations of spin dependent quantities.

*ivady.viktor@wigner.mta.hu

CONTENTS

I. INTRODUCTION

In the last decades considerable efforts have been made to utilize fundamental aspects of quantum mechanics in various visionary applications, such as quantum information processing and quantum computation.[1] The conceptual building block of these revolutionary applications is the quantum bit (qubit), the simplest possible quantum system that includes only two levels. In practice, the levels implementing the qubit states must be isolated from the environmental degrees of freedom and at the same time they must remain controllable via different external means. Simultaneous fulfillment of these criteria causes one of the major challenges in qubit implementations.

Qubits have been already demonstrated in a broad range of physical systems.[1] Point defect based quantum bits in semiconductors are among the most recent realizations[2–7], where generally the spin of a paramagnetic point defect or associated paramagnetic nuclei gives rise to the quantum states that may be manipulated by electric and magnetic fields, microwave irradiations, and optical means.[3] Due to the special characteristics of the point defect qubits and the properties of the semiconducting host material, the existing point defect quantum bits are well isolated from their environment[3,7]. This leads to observations of generally long coherence times[3,8] and qubit operation even at room temperature[9–11]. For example, in isotope engineered high purity diamond sample the coherence time can exceed a millisecond at room temperature.[9] These attributes together with the possibility of magneto-optical control make point defect qubits, including single or ensemble of isolated qubits, highly promising for numerous applications. For instance, point defect qubits created in nanocrystals or close to the surface of nano fabricated thin film samples can be utilized as atomic-scale temperature[12], electric field[13], and strain[14] sensors, as well as magnetic resonance probes[15–17] that are about to revolutionize nanoscale metrology. Ensembles of point defects qubits in larger samples can be used to greatly increase the sensitivity of microscale room temperature sensors[18,19] and gyroscopes[20,21] with some of them readily integrable in existing semiconducting electric devices. Quantum optics devices are intensively studied for quantum information processing applications[22,23] and for testing fundamental aspects of quantum entanglement. Indeed, the loophole-free Bell test was first demonstrated by point defect qubits[24]. Silicon based quantum computation maybe be realized by using single point defect spins and quantum dots.[1,5,25] Furthermore, point defect qubits can be used to polarize nearby nuclear spins[26,27], thus ensembles of these nuclear polarization sources can lead to the hyperpolarization of the host material that may be utilized in nuclear magnetic resonance and imaging to enhance sensitivity by

orders of magnitudes[28].

The quality of the point defect qubits, i.e. the fidelity of spin state manipulation and read-out and the decoupling from the environment degrees of freedom, determines the capabilities and limitations of the potential applications. The quality of the point defect qubits relies on the other hand on the properties of the semiconductor host material and the point defect that give rise to the isolated electron or nuclear spin states. Consequently, understanding and engineering point defect qubits and their applications often translate to material science and material engineering problems. Considering the vast diversity of these fields, there are many potential directions for future point defect qubit research.

In this respect, computational studies play an essential role in material science because of the detailed physical picture they provide and due to their significant predictive power. First principles electronic structure calculations have greatly contributed to the quantitative understanding of point defect qubit related materials, leading to the fast development of the field. On the other hand, the emerging research directions generally require the development of novel computational methods and tools. Specifically, point defect qubit studies require high precision electronic structure calculations of ground and excited state properties, as well as all kinds of derived spin dependent properties at various environmental conditions.

Here, we report on recent developments and applications of first principles calculations of point defects electronic structure and spin related quantities for solid-state qubits in semiconductors. By going through the recent achievements in this area, we highlight required additional developments and point out possible new directions that can further increase the predictive power and area of applications of the computational methods.

II. PHYSICS OF POINT DEFECT QUBITS

There are two major classes of point defect qubits in semiconductors. In the first type of qubits, electron and nuclear spins of shallow donors, such as phosphor and bismuth, in silicon are manipulated through electrical-gates (quantum dots).[5,8,25,29,30] Spin-orbit and hyperfine interactions play a crucial role in the physics and applications of these qubits. The corresponding spin dependent quantities can be calculated from first principles as we discuss in Sec. IV.

In this section, we focus on the second class of point defect qubits, i.e. deep-level high spin state color centers in wide band gap semiconductors whose spin can be manipulated by optical means. Using confocal microscopy techniques, it is possible to excite and collect photons from defects in a volume of $\mathcal{O}(10\ \mu\mathrm{m}^3)$ of a semiconducting sample.[31] For low point defect concentration the examined volume may contain only a few, ultimately one single color center. Individual color centers in semiconductors that exhibit fast bound-to-bound optical transition may implement single photon emitters that often operate even at room temperature.[22,32–34] Optically controllable point defect qubits form a special class of single photon emitters. Due to this duality, point defect qubits exhibit great potential in a broad range of quantum information processing and sensing applications.[2,3,7,35]

For qubit implementation, a color center must fulfill additional requirements: it must form high spin ground and/or excited state, the electron spin must exhibit long coherence time, and the luminescence of the defect should be spin dependent. The latter requirement enables optical initialization and read-out of a point defect qubit. Additionally, applying external magnetic field and microwave irradiation, full control of the point defect spin states can be achieved. As an example, in the following we consider the most thoroughly investigated room temperature point defect qubits in semiconductors, namely 1) the negatively charged nitrogen substitutional-vacancy complex in diamond (NV center)[9,36,37], 2) the neutral silicon-carbon double vacancy in SiC polytypes (divacancy)[10,38], and 3) the isolated negatively charged silicon vacancy in SiC polytypes (silicon vacancy)[11,39]. SiC is a technologically mature polytypic material with polytypes of complicated stacking sequences in general, thus SiC hosts often give rise to symmetrically non-equivalent configurations of a considered point defect. Consequently, divacancy and silicon vacancy qubits represent families of several distinguishable configurations with slightly different characteristics and varying potential for applications rather than a single qubit.[40]

NV center and divacancy exhibit qualitatively similar electronic structure[47], therefore we dis-

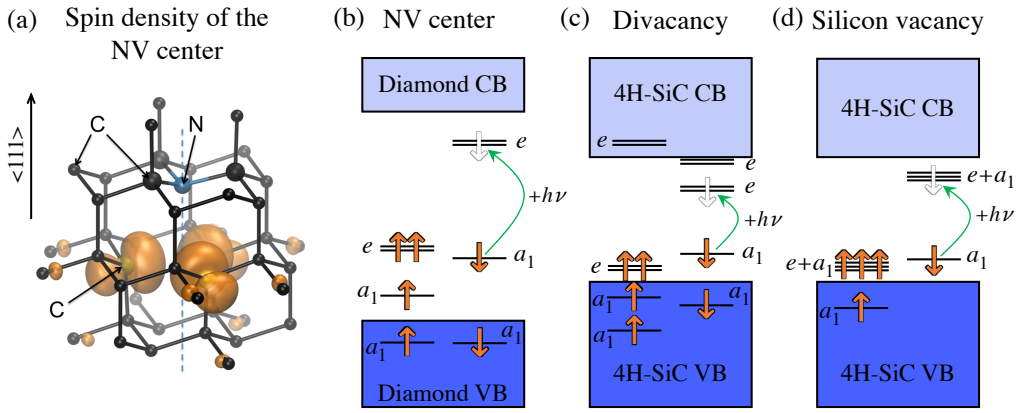

FIG. 1. (a) Structure and spin density of the NV center in diamond, and (b)-(d) Kohn-Sham electronic structure of the NV center in diamond and divacancy and silicon vacancy in 4H-SiC, respectively. Green arrows represent the lowest energy optical transition in the single particle picture. The Kohn-Sham electronic structures were obtained by convergent HSE06 hybrid functional calculations.[41–43]

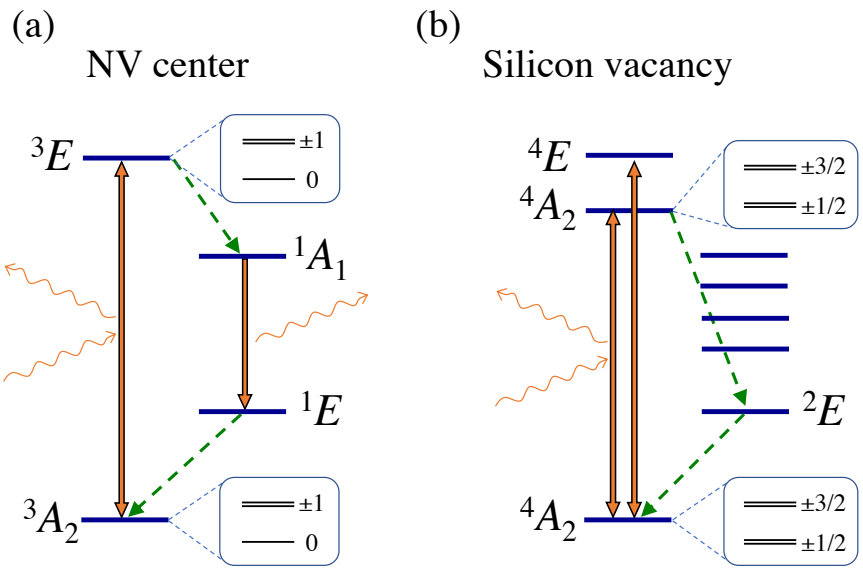

FIG. 2. Low energy many particle states of (a) the NV center in diamond[44,45] and (b) silicon vacancy in SiC[46].

cuss the physics of these defects together. The four (six) dangling bonds of the NV center (divacancy) form two a_1 and one e (two a_1 and two e) single particle states that occupied by six (six) electrons. According to *ab initio* density functional theory calculations (DFT)[41,42,47,48], a fully occupied lower lying a_1 state and an e state, occupied by two electrons, appear in the lower part of

the band gap for both defects, see Fig. 1(b)-(d). In the case of divacancy, an empty e state can also be found close to the conduction band edge, however, it has negligible effect on the properties of the defect. Due to the half occupied e state above the a_1 state, both defects exhibit a spin-1 ground state of ${}^3A_2$ symmetry, see Fig. 2(a) for the NV center. Relativistic effects, mostly dominated by the dipolar coupling of the unpaired electron spins, split the substates of the triplet ground states, see Fig. 2(a), by ≈ 2.9 and ≈ 1.3 GHz for the NV center[49] and divacancy[50], respectively. Spin conserving optical excitation can drive the system into the lowest optically exited state of ${}^3E$ symmetry. In single particle picture, an electron is promoted from the a_1 state to the lowest e state, see Fig. 1(b)-(d). Note that this electronic configuration gives rise to a dynamic Jahn-Teller system with strong electron-phonon interaction and effective C_{3v} symmetry when the axis of the pair defect is parallel to the high symmetry axis of the host material. Due to the spin-orbit and spin-spin dipolar interactions, the ${}^3E$ state exhibits a complicated fine structure at low temperature[51–53]. At higher temperature, the spin-orbit interaction and off-axis components of the spin-spin zero-field-spitting interaction average out due to the motion of the atoms.[54] The high temperature fine structure of the ${}^3E$ state resembles the fine structure of the ground state, i.e. it can be parameterized by the axial zero-filed-splitting parameter D.[54]

The spin selectivity of the optical transition can be explained through shelving states that appear between the lowest optically excited state and the ground state. The generally accepted many particle electronic structure of the NV center and divacancy can be seen in Fig. 2(a). It includes a ${}^1A_1$ and a ${}^1E$ singlet states between the triplet excited and ground states.[44,45] Transitions between the singlet and triplet branches can occur due to the interplay of local vibrational modes, inter system crossing of the energy levels, and off-axis spin-orbit coupling.[44,45,55] Due to the latter interaction, different spin states of the ${}^3E$ excited state exhibit different non-radiative decay rates through the singlet states. Consequently, different spin states have different lifetime and different luminescence intensity as well. By applying microwave irradiation to drive spin state transitions, this phenomenon allows optical detection of magnetic resonance (ODMR) which is a key technique for optical spin state read-out of point defect qubits.[56] Additionally, through the non-radiative transitions between the triplet and singlet states, there is nonzero rate for the $m_S = \pm 1 \rightarrow m_S = 0$ transition. Therefore, it is possible to highly polarize the electron spin of the point defect in the $m_S = 0$ state by repeated optical excitation.[2,3]

The dangling bonds of silicon vacancy form two a_1 and one e single particle states that all appear in the band gap of 4H-SiC[57], see Fig. 1(d). This defect has near t_d symmetry, thus the

higher lying a_1 and the e states are nearly degenerate and splitted only by 80 meV according to recent DFT calculations[43]. In the negative charge state, the single particle states are occupied by five electrons that give rise to spin-3/2 ground (^{4}A$_2$) and optically excited (^{4}A$_2$ and ^{4}E) states, see Fig. 2(b). In contrast to the NV-center and divacancy, the ground state fine structure of silicon vacancy exhibits a zero-field-splitting of only $\mathcal{O}(10$ MHz$)$[43], while the excited state fine strucutre exhibits a splitting in the order of 100 MHz[58]. There are several possible doublet shelving states between the quartet ground and excited states.[46] According to group theory considerations[46], the non-axial spin-orbit interaction can only connect the ground and excited $^4A_2$ states trough a ^2E doublet state, see Fig. 2(b). Through this spin selective non-radiative decay path the spin of silicon vacancay qubit can be initialized in the $m_{\rm S} = \pm 1/2$ spin subspace.[46]

Beside the electron spin of point defects, nearby nuclear spins, interacting with the point defects through the hyperfine coupling, can also be utilized as quantum bits. As nitrogen has only paramagnetic isotopes, the NV center always form a coupled electron spin-nuclear spin two qubit system.[26,59] The host semiconductor may also contain nuclear spins that can be used to realize hybrid qubit systems.[31] Diamond contains 1.07% spin-1/2 ^{13}C, while SiC contains 1.07% spin-1/2 ^{13}C and 4.68% spin-1/2 ^{29}Si isotopes in natural abundance.

Spin-orbit interaction at the defect site and in the bulk, and dipolar coupling of nuclear and other point defect spins are responsible for spin relaxation mechanism in these qubit implementations. Purification of the host material from paramagnetic isotopes and point defects were successfully used to elongate relaxation and coherence times.[9,38]

III. FIRST PRINCIPLES ELECTRONIC STRUCTURE CALCULATIONS

Theoretical characterization of point defects qubits and first principles calculations of spin coupling parametes depend crucially on the outcomes of the underlying electronic structure calculations. Therefore, it is essential to understand the capabilities and limitations of the latter before we discuss the results of the calculations. Unfortunately, due to the large structural model, which is generally needed for the accurate description of single point defects in bulk semiconductor hosts, one must always compromise between the accuracy and computational efficiency. DFT is the most widely used method in the field. However, there are numerous attempts to use more sophisticated Green's function and wavefunction based methods for point defect qubit calculations, see later in this section.

Let us therefore shortly review the most relevant electronic structure theories used in ground and excited state calculations of point defect qubits. As a first basic approximation, one generally assumes that the wavefunctions of the nuclei and the electrons can be separated (the Born-Oppenheimer approximation). Relying on this approximation, the electronic structure problem can be solved for every fixed arrangement of the atomic nuclei. Note, however, that when the point defect qubit has Jahn-Teller unstable state(s), for instance, the excited state of the NV center and divacancy, one must go beyond the Born-Oppenheimer approximation, see section IV F.

A. Ground state methods

DFT[60,61] in the Kohn-Sham[62,63] and generalized Kohn-Sham[64] formalisms are the most frequently used methods for the ground state electronic structure calculation of cluster or supercell models of point defects in semiconductors. In these two formalisms, the Schrödinger problem of many-electron system is mapped onto the problem of auxiliary non-interacting and partially interacting Kohn-Sham particles, respectively. The mapping is constructed so that the auxiliary system reproduces the one particle density and the total energy of the considered system.[61,63] Exact calculations require the definition and calculation of the exchange-correlation energy term as a functional of the density. The exact definition of the exchange-correlation energy functional is not known in general, thus it is approximated in practice.[61,63]

In first principles studies of point defects qubits in semiconductors, the most widely used approximate exchange-correlation functionals are the PBE[65] functional and the HSE06[66,67] hybrid functional. The latter functional models a partially interacting system in the framework of generalized Kohn-Sham scheme[64]. HSE06 hybrid functional includes the calculation of the exact exchange energy of the Kohn-Sham particles[66,67], which makes this functional computationally more demanding. In conventional semiconducting hosts, HSE06 hybrid functional provides the most accurate results for bulk and sp-point defect related quantities in general[68–70], as we discuss later in this paper. There are two main reasons for the improved performance of HSE06: 1) it exhibits a derivative discontinuity in the exchange correlation potential[71] that remedies the band gap underestimation problem of semi-local Kohn-Sham DFT functionals in conventional semiconductors[68,72] and 2) localized defect states often satisfy the generalized Koopman's theorem[69,73] thus there is no self-interaction for the auxiliary particles occupying the defect states[74]. On the other hand, when impurities with partially filled d-orbitals are considered, the HSE06 functional tends to fail

in producing reliable results.[75,76]

Supercell structural models of point defects with periodic boundary conditions are the most often used approaches to investigate point defect qubits in semiconductors. In such models, plane wave basis set is the most suitable for expressing Kohn-Sham single particle wavefunctions in the inter-atomic region. Interaction with the atomic cores, including the potential of the nuclei and the core electrons, is described either by pseudo potentials or by the projector augmented wave (PAW) method[77] in most of the calculations. The latter enables the calculation of atomic core related quantities, such as spin-orbit interaction and hyperfine Fermi contact term with all-electron accuracy, see later in section IV.

Convergence and numerical accuracy are always important aspects of first principles DFT calculations. The most relevant technical parameters that determine the accuracy of the calculations are the supercell size, Brillouin zone sampling, basis set, and the force or energy criteria used for the structural optimization. As will be shown in Sec. IV, in the case of spin coupling parameter calculations, often very high numerical accuracy is needed. Recently, thorough numerical tests, including ground state, optical, and hyperfine parameters calaucltaions were carried out for the divacancy qubit in 4H-SiC in Refs. [42] and [78].

From the ground state spin density and Kohn-Sham particle wavefunctions most of the relevant ground state spin dependent properties can be approximately calculated, see section IV.

B. Excited state methods

As we have seen in section II, spin state initialization and read-out can be implemented through the optical cycle of point defect qubits. This process is determined by the electronic structure of the point defects, especially, on the excited state spectrum and the coupling and inter-system-crossing of different states. There are several wave-function based quantum chemistry approaches that can provide such spectrum from first principles, however, majority of these methods are applicable only for small systems. Large point defect models with the periodic boundary conditions are challenging for such calculations. The most widely used approaches today apply computationally less demanding DFT based methods, for instance, the constrained occupation DFT method. Limited accuracy of this method however motivated development of efficient, still more advanced computational approaches.

1. *Constrained occupation DFT*

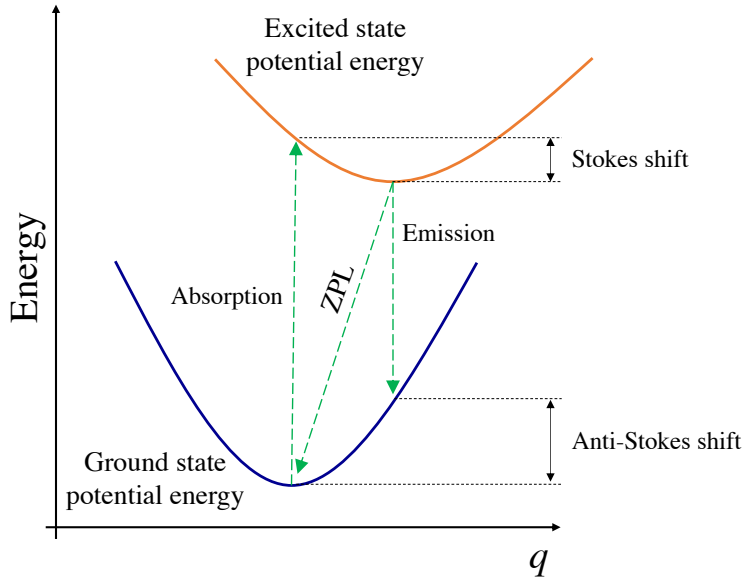

FIG. 3. Schematic diagram of the configuration coordinate diagram of a point defect's ground and excited states. Green arrows show the most relevant phonon assisted and zero-phonon (ZPL) optical transitions.

In constrained occupation DFT[79], the total energy of a point defect excited state configuration is approximated by the DFT total energy of a Kohn-Sham system, where one of the occupied Kohn-Sham defect states is depopulated, while a higher lying unoccupied Kohn-Sham state is populated, see Fig. 1(b)-(d). The constrained occupation of the orbitals is kept fixed during the self-consistent solution of the Kohn-Sham equations. Note that structural optimization of the systems is still possible within this approach as the total energy is well-defined. Consequently, besides the absorption energy, which requires the same ground and excited state atomic configuration in the Franck-Condon approximation, the emission and zero-phonon energy, as well as the Stokes and anti-Stokes shifts can be calculated in the constrained occupation DFT, see Fig. 3. In Table I, one can see these quantities for the NV center. Remarkable accuracy was reported for the optical properties calculated by HSE06 functional[79]. For more details on first principles calculation of optical properties see Ref. [80].

The constrained occupation DFT inherently assumes that the Kohn-Sham orbitals of the defect states have a true physical meaning, thus the change of the occupancies can indeed mimic a realistic excitation process. According to the generalized Koopmans' theorem[82,83], or in other context

TABLE I. Optical properties of the NV center from first principles constrained occupation DFT. Theoretical values were calculated by PBE and HSE06 functionals in Ref. [79]. Experimental values are reported in Ref. [81].

	PBE	HSE06	Exp.
Absorption energy	1.910	2.213	2.180
Zero-phonon-line energy	1.706	1.955	1.945
Emission energy	1.534	1.738	1.760
Stokes shift	0.204	0.258	0.235
anti-Stokes shift	0.172	0.217	0.185

the ionization potential theorem[71,84], this is only fulfilled for the highest occupied state when its Kohn-Sham single particle energy is equal to the negative of the ionization potential,

$$\varepsilon_{\text{ho}} + \Delta\varepsilon_{\text{cc}} = -\left(E_N - E_{N-1} + \Delta E_{\text{cc}}\right), \tag{1}$$

where ε_{ho} is the energy of the highest occupied Kohn-Sham orbital and E_N is the total energy of the N electron system. Note that due to the periodic boundary condition, finite size effects can be strong for charged supercells, both in terms of the Kohn-Sham eigenenergies and the total energies, and they must be corrected by appropriate charge correction terms, $\Delta\varepsilon_{\text{cc}}$ and ΔE_{cc}, respectively.[85]

Recent theoretical studies[69,73] demonstrated that defect states described by HSE06 functional often fulfill Eq. (1). Thus the constrained occupation DFT may describe realistic excitation processes, which explains the remarkable accuracy seen in Table I.

The constrained occupation DFT describes excitation processes in terms of a single Slater determinant of the Kohn-Sham particles. The constraint occupation DFT method, however, often fails to provide accurate total energies of states that are highly correlated, or in the language of Hartree-Fock theory, are multideterminant in nature. Open shell singlet states fall into this category. This limitation greatly hinders the computational description of the spin selective non-radiative decay process that may include transition through open shell singlet states.

2. *Excited state calculation beyond constrained occupation DFT*

In order to calculate highly correlated states, several alternative methods have been proposed and tested for the NV center in diamond. Parameters of the excited state spectrum obtained by

TABLE II. Parameters of the electronic structure of the NV center in diamond as calculated by different theoretical approaches.

Method	${}^3E \rightarrow {}^3A_2$	${}^1A_1 \rightarrow {}^1E$	${}^3E \rightarrow {}^1A_1$
GW+BSE[a]	2.09	0.59	1.10
CI on $C_{42}H_{42}N^-$ [b]	1.93	1.43	-0.1
Ext. Hubb. + DFT par.[c]	2.38	0.62	1.35
Ext. Hubb. + GW fit.[d]	2.0	0.96	0.6
Experiment	1.945[x]	1.19[y]	≈0.4[z]

[a] Reference [86], [b] Reference [87], [c] Reference [88], [d] Reference [89], [x] Reference [81], [y] Reference [90], [z] Reference [91],

different first principles methods are summarized and compared with the experimental values in Table II.

The most widely use method to describe excited state phenomena in solids is the GW approximation to the Hedin equations[92] in the framework of many-body perturbation theory. The method can be combined with the colution of the Bethe Salpeter equation (BSE)[93] to include electron-hole interactions and to describe singulet states. GW+BSE method was applied in simulations of the NV center by Ma *et al.* in Ref. [86], where three singlet states, ${}^1E$, ${}^1A_1$, and ${}^1E'$ states, were found between the triplet ${}^3E$ excited and ${}^3A_2$ ground states. This result is in contradiction with the currently accepted energy structure of the NV center discussed in section II. Furthermore, the calculated 0.59 eV ZPL energy of the ${}^1A_1 \rightarrow {}^1E$ transition is approximately half of the experimental value, suggesting that G_0W_0+BSE method fails to accurately describe important static correlation effects in the singlet states.

Quantum Monte Carlo configuration interaction (QMC CI) calculation on small cluster models[87] and generalized Hubbard model based approaches[88,89], on the other hand, are able to qualitatively reproduce the accepted energy level structure of the NV center, i.e. they predict only two shelving states that can be connected to the nonradiative decay process of the NV center, see Table II.

In the QMC CI approach on a $C_{42}H_{42}N^-$ cluster, Delaney *et al*. in Ref. [87] reported that the higher lying ${}^1A_1$ shelving state appears slightly above the ${}^3E$ states. This result suggests higher energy inter system crossing and thus lower decay rate. Furthermore, the ${}^1A_1 \rightarrow {}^1E$ transition

energy is overestimated, see Table II. The discrepancies can most probably be attributed to the very small cluster model used in the calculations.

In the third-type of approaches extended Hubbard model Hamiltonians were diagonalized for the electrons occupying the dangling bonds of the NV center,

$$H = \sum_{ij\sigma} t_{ij} c^{\dagger}_{i\sigma} c_{j\sigma} + \sum_{i} U_i n_{i\uparrow} n_{i\downarrow} + \frac{1}{2} \sum_{i \neq j, \sigma\sigma'} V_{ij} n_{i\sigma} n_{j\sigma'} + \frac{1}{2} \sum_{ijlm, \sigma\sigma'} X_{ijlm} c^{\dagger}_{i\sigma} c^{\dagger}_{j\sigma'} c_{m\sigma'} c_{l\sigma}, \quad (2)$$

where i, j, l, and m are dangling bond indexes, σ and σ' are the spin indexes, c, $c^{\dagger}$, and $n^{\dagger}$ are the annihilation, creation, and number operators, t is the hopping and ionic term, U and V are the intra and intersite Coulomb repulsion, and X is the exchange interaction term. In Ref. [88], Ranjbar *et al.* calculated the hopping and interaction parameters from the defect orbitals obtained by DFT calculations with B3LYP functional[94] on a $C_{71}H_{85}$ cluster. This method somewhat overestimates the ${}^3E \rightarrow {}^3 A_2$ transition energy, while substantially underestimates the ${}^1A_1 \rightarrow {}^1 E$ ZPL energy, see Table II. In Ref. [89], Choi *et.al*. applied a different approach to paramaterize a Hubbard Hamiltonian that neglected the exchange interaction term in Eq. (2). In order to determine U and V, they compared quasi particle energies as obtained from GW calculation and from the diagonalization of the Hubbard Hamiltonian. Through this fitting, the screening effect of the delocalized semiconductor states was included to some extent. Despite omitting the exchange interaction term, today this approach provides the most accurate excited state spectrum parameters, indicating the importance of taking screening effect into account.

As we have seen in this section both the local static correlation effect of the dangling bonds and the dynamic screening effects of the delocalized electronic states must be accounted for properly to describe the open-shell singlet states of point defect qubits. To support the rapidly growing field of point defect qubits studies by *ab initio* exited state electronic structure calculations, a practical method, that can combine many-body perturbation theory based methods with wavefunction based method on a solid theoretical ground, is highly desired.

IV. FIRST PRINCIPLES SPIN COUPLING PARAMETER CALCULATION

A. g-tensor

Magnetic field is traditionally used to control the splitting of the spin states of point defect qubits, and *vice versa*, it is possible to detect magnetic field variations by measuring the splitting

of the spin states. The spin Hamiltonian operator for defect spins with $S \leq 1$ and for negligible first order ground state spin-orbit interaction can be written as

$$\hat{H}_{\text{Zeeman}} = \mu_{\text{B}} \mathbf{B} \mathbf{g} \hat{\mathbf{S}}, \tag{3}$$

where μ_{B} is the Bohr magneton, $\mathbf{B}$ is the magnetic field vector, $\hat{\mathbf{S}}$ is the electron spin vector operator, and the $\mathbf{g}$ is the g-tensor that includes different higher order relativistic material dependent contributions to the g_e g-factor of the free electron. The Cartesian elements of the g-tensor can be obtained from the second derivative of the relativistic many electron energy E, as[95]

$$g_{ab} = \frac{1}{\mu_{\text{B}}} \frac{\partial^2 E}{\partial B_a \partial S_b}\bigg|_{B=0,S=0}, \tag{4}$$

which give rise to three additional non-negligible terms beside the $\hat{H}_{\text{Z-free}}$ Zeeman term of the free electron,

$$\hat{H}_{\text{Zeeman}} = \hat{H}_{\text{Z-free}} + \hat{H}_{\text{Z-KE}} + \hat{H}_{\text{Z-SO}} + \hat{H}_{\text{Z-SOO}}, \tag{5}$$

where $\hat{H}_{\text{Z-KE}}$ is the electron Zeeman kinetic energy correction, and $\hat{H}_{\text{Z-SO}}$ and $\hat{H}_{\text{Z-SOO}}$ are the spin-orbit and spin-other-orbit corrections to the Zeeman energy. The definition of these terms can be found in the literature, for instance in Ref. [95–97]. The effective g-tensor of the system is defined as

$$\mathbf{g} = g_e \mathcal{I} + \Delta\mathbf{g}_{\text{Z-KE}} + \Delta\mathbf{g}_{\text{Z-SO}} + \Delta\mathbf{g}_{\text{Z-SOO}}, \tag{6}$$

where $\mathcal{I}$ is the 3×3 identity matrix, and $\Delta\mathbf{g}_{\text{Z-x}}$ are the corresponding correction tensors.

Implementations that are suitable for point defect g-tensor calculations in periodic models were provided by Sebastiani *et al.* in Ref. [98] and Pickard *et al.* in Ref. [97]. In the former approach pseudo potentials were used without correction terms in the core region that resulted in limited applicability of the method. Later, this limitations was relaxed by extending the method in Ref. [99]. On the contrary, Pickard *et al.* in Ref. [97] used gauge including projector augmented wave approach[100] (GIPAW), which allowed for all-electron g-tensor calculations. Later, implementations using atomic orbitals in periodic boundary conditions were also presented.[101] g-tensor calculations were recently applied in the identification of the microscopic configuration of the nitrogen substitutional-silicon vacancy pair defect in different polytypes of SiC.[102] This new family of spin-1 point defects was recently suggested as a potential new platform for implementing point defect qubit in technologically mature SiC hosts.[103].

So far we considered only bi-linear terms in the Zeeman spin Hamiltonian. For defects with $S > 1$, higher order magnetic field interaction terms are possible[96,104]. In Table III, we collected

TABLE III. Possible electron spin-electron spin and electron spin-magnetic field terms in the spin Hamiltonian.[104] Here, $\hat{S}$ represents any linear combination of the spin Cartesian operators, while B represents any linear combination of the Cartesian magnetic field components.

S	Terms				
$\frac{1}{2}$	$\hat{S}B$				
1	$\hat{S}B$	$\hat{S}^2$			
$\frac{3}{2}$	$\hat{S}B$	$\hat{S}^2$	$\hat{S}^3B$		
2	$\hat{S}B$	$\hat{S}^2$	$\hat{S}^3B$	$\hat{S}^4$	
$\frac{5}{2}$	$\hat{S}B$	$\hat{S}^2$	$\hat{S}^3B$	$\hat{S}^4$	$\hat{S}^5B$

the possible higher order magnetic field interaction terms up to $S = 5/2$. Note, that Table III does not contain higher order terms in B. Such terms are also possible, however, most often they can be safely neglected.[104]

Theoretical formulas for the higher order interaction terms can be found in the literature[104,105], however, less attention has been paid to the implementation and calculation of corresponding higher order g-tensor parameters so far. On the other hand, in recent experiment on the spin-3/2 silicon vacancy qubits in 4H-SiC forbidden electron spin transitions were observed in the ODMR spectrum.[106] To explain this result, higher order $\hat{S}^3B$ like terms had to be taken in the considerations. The g-tensor elements corresponding to these third order terms were found to be considerable, i.e. $g_{3\perp} + g_{3\parallel} \approx 1.0$ and $g_{3\perp} - g_{3\parallel} \approx 0.2$. These results indicated that implementations of higher order magnetic field interaction term calculation may be desirable in the future to understand forbidden transitions.

B. Spin-spin contribution to zero-field splitting

Due to intra-defect interactions, the spin sublevels of the point defect qubits may split even at zero magnetic field. There are two major contributions to the, so-called, zero-filed-splitting (ZFS): the spin-spin and the spin-orbit dipole interactions. In this section we discuss first principles calculations of the former interaction, which is generally the most relevant interaction in the ground state of the considered solid state qubits..

When a point defect has more than one unpaired electron, each pair of the electrons spins $\hat{\mathbf{S}}_i$

and $\hat{\mathbf{S}}_j$ interact thorough the dipole-dipole interaction, described by the following Hamiltonian,

$$\hat{H}_{\mathrm{SS},ij} = \frac{\mu_0}{4\pi} g_e^2 \mu_\mathrm{B}^2 \left(\frac{\hat{\mathbf{S}}_i \hat{\mathbf{S}}_j}{r^3} - \frac{3\left(\hat{\mathbf{S}}_i \mathbf{r}\right)\left(\hat{\mathbf{S}}_j \mathbf{r}\right)}{r^5} \right), \tag{7}$$

where $\mathbf{r}$ is the vector between the two electron spins, $r = |\mathbf{r}|$, and μ_0 is the vacuum permeability. Note that, for simplicity the g-tensor of the electron spin is replaced with the g_e g-factor of the free electron.[104] The spin-spin contribution to the zero-field-splitting spin Hamiltonian can be obtained by introducing the total spin operator vector, $\hat{\mathbf{S}} = \sum_i \hat{\mathbf{S}}_i$, and integrating over the spatial degrees of freedom. Note that this is possible when the spatial and spin wavefunctions are separable, i.e. no spin-orbit interaction mixes these two degrees of freedom. The spin Hamiltonian can be written as

$$\hat{H}_{\mathrm{SS,\,ZFS}} = \hat{\mathbf{S}}\mathbf{D}\hat{\mathbf{S}}, \tag{8}$$

where $\mathbf{D}$ is the 3×3 zero-field-splitting tensor. Components of the zero-field-splitting tensor can be calculate from the two particle spin density matrix $\rho_2(\mathbf{r}_1, \mathbf{r}_2)$ as,

$$D_{ab} = \frac{1}{2}\frac{\mu_0}{4\pi} g_e^2 \mu_\mathrm{B}^2 \int \rho_2(\mathbf{r}_1, \mathbf{r}_2) \frac{r^2\delta_{ab} - 3r_a r_b}{r^5} d\mathbf{r}_1 d\mathbf{r}_2, \tag{9}$$

where r_a and r_b are the Cartesian coordinates of $\mathbf{r} = |\mathbf{r}_1 - \mathbf{r}_2|$. In axial symmetric cases the splitting of the spin states can be parameterized by a single parameter, $D = \frac{3}{2}D_{zz}$, and the ZFS spin Hamiltonian simplifies to

$$\hat{H}^{\text{axial sym.}}_{\mathrm{SS,\,ZFS}} = D\left(\hat{S}_z^2 - \frac{S\left(S+1\right)}{3}\right), \tag{10}$$

where S is the total spin and S_z is the eigenvalue of the component along z quantization axis..

The two particle spin density matrix can be obtained in different wave function based approaches, as it is generally carried out in quantum chemistry calculations for molecules[107]. However, it is only approximated in point defect calculations with periodic boundary conditions[108]. In DFT only density related quantities can be determined in a consistent way. The density matrix can be approximated by using the Slater determinant of the Kohn-Sham eigenstates of the considered system. This approximation is suitable only when the ground state wave-function is accurately represented by a single Slater determinant[108,109]

$$D_{ab} = \frac{1}{2}\frac{\mu_0}{4\pi}\frac{g_e^2\mu_\mathrm{B}^2}{S\left(2S-1\right)} \sum_{i>j}^{\text{occupied}} \chi_{ij} \int \left|\Phi_{ij}(\mathbf{r}_1, \mathbf{r}_2)\right|^2 \frac{r^2\delta_{ab} - 3r_a r_b}{r^5} d\mathbf{r}_1 d\mathbf{r}_2, \tag{11}$$

where $\Phi_{ij}(\mathbf{r}_1, \mathbf{r}_2) = \frac{1}{\sqrt{2}} \left(\phi_i(\mathbf{r}_1) \, \phi_j(\mathbf{r}_2) - \phi_j(\mathbf{r}_1) \, \phi_i(\mathbf{r}_2) \right)$ the Slater determinant of Kohn-Sham states i and j and χ_{ij} is either 1 or -1 for KS states of the same or different spin channels, respectively. Note that in DFT the Kohn-Sham states are not spin restricted, i.e. the states in the two spin channels are independent from each other. Consequently, not only the unpaired Kohn-Sham states but also the rest of the occupied states can contribute to the spin density and the ZFS[108,109]. In order to account for these effects, the summation in Eq. (11) includes all pairs of the occupied states.

To the best of our knowledge, the first implementation and point defect calculations were carried out by Rayson *et al.* in Ref. [109] and [108]. In the latter publication an efficient implementation was presented for the plane wave basis set, which was later utilized in other publications too[110,111]. In all of these early implementations pseudopotentials and pseudo wavefunctions were used. The theory of Rayson *et al.* was recently extended to the PAW method to include corrections from the core region[112,113].

We would like to draw attention to the fact that the dipole-dipole interaction is long ranged, i.e. it goes with $1/r^3$, thus the finite size effect can be present in periodic supercells. Biktagirov *et al.* in Ref. [113] observed notable effect for point defects in diamond and cubic 3C-SiC. Note that ZFS is a tensor quantity, thus the interaction with the periodic images depends not only on the distances but on the arrangement of the replicas, or equally, on the shape and symmetry of the supercell. To investigate these important aspects that influence the numerical accuracy and to propose possible correction schemes, additional studies are required.

Recently, the ground state ZFS tensor calculations were successfully applied in point defect configuration identification studies[42,43,103], where 1-20% error were observed when the values are compared with experimental results, see Table IV. In all of these applications PBE exchange-correlation functional was used. Note that the results obtained from pseudo wavefunctions without PAW contributions compare best with the experimental values. This surprisingly good results must be a consequence of error cancellations in these calculations.[111] Note also that the current implementations may not be suitable for defects with $S \geqslant 2$, where higher order terms are expected, see Table III, and when the g-tensor deviates considerably from $g_e \mathcal{I}$ of the free electron[104].

ZFS of point defect qubits is a key quantity to measure variations of the external degrees of freedom. Recently, pressure[110,111], strain[116], electric field[114], and temperature dependence[110] of the ZFS were successfully studied by first principles calculations.

So far less attention has been paid to the excited state ZFS calculations, where additional con-

TABLE IV. First principles and experimental ground state ZFS values D of selected point defects that are used or proposed as qubits in semiconductors. ONCV, PAW-ps, and PAW superscripts stand for calculations with norm-conserving pseudopotentials, PAW potential with only pseudo wavefunction contributions to the ZFS, and PAW potential with PAW core corrections to the ZFS, respectively. All values are given in GHz.

Host	defect	D^{ONCV}	$D^{\text{PAW-ps}}$	D^{PAW}	$D^{\text{exp.}}$
diamond	NV^-	3.03[a]	2.90[a], 2.854[b]	3.08[c]	2.88[d]
4H-SiC	hh divacancy	1.682[a]	1.387[a], 1.358[e]	–	1.336[f]
4H-SiC	V_{Si}^- at the k-site	–	0.0333[g]	–	0.035[h]
3C-SiC	$N_C V_{Si}^-$	–	1.409[i]	1.74[c]	1.303[i]

[a] Reference [111], [b] Reference [110], [c] Reference [113], [d] Reference [56], [e] Reference [114], [f] Reference [40], [g] Reference [43], [h] Reference [115], [i] Reference [103]

siderations are required. As we mentioned in section II, ZFS tensor can be obtained only when the spin and spatial degrees of freedom are separable, i.e. spin-orbit interaction is negligible, and the considered states can be described by a single Slater determinant. None of these conditions are satisfied in the low temperature fine structure of the ${}^3E$ optically excited state of the NV center[44,55] and divacancy[53], thus spin-spin coupling alone cannot describe the low temperate fine structure. On the other hand, according to the accepted theory of the ${}^3E$ states of these defects, at high temperature the spin-orbit interaction and non-axial component of the spin-spin interaction averages out due to the atomic motion of the dynamic Jahn-Teller excited state configuration[55], and thus one can obtain states that are good eigenstates of $\hat{S}_z$ and $\hat{S}_z^2$. The ZFS of the NV center and divacancy qubits can be approximated by Kohn-Sham orbitals in constrained occupation DFT and subsequent symmetrization of the $\mathbf{D}$ matrix to mimic the motion averaging and obtain effective C_{3v} symmetry.

In Table V, we collected the results of excited state ZFS calculations using PAW pseudowavefunctions obtained by PBE exchange correlation functional.[117] Except for the NV center in diamond, the theoretical values substantially overestimate the experimental ones. A possible source of this discrepancy can be the neglect of electron-phonon coupling and the vibrational part of the wavefunction. These results as well as the enormous temperature dependence of the excited state ZFS of silicon vacancy[58] evidence the need for extending the theory of excited state ZFS

TABLE V. First principles and experimental excited state ZFS values D of selected point defects qubits. PAW-ps denotes calculations of PAW potential with only pseudo wavefunction contributions to the ZFS. All values are given in GHz unit.

Host	defect	$D^{\text{PAW-ps}}$	$D^{\text{exp.}}$
diamond	NV^-	1.71[a]	1.43[b]
4H-SiC	hh divacancy	1.33[a]	0.84[c]
4H-SiC	V_{Si}^- at the k-site	2.19[a]	0.215-0.503[d]

[a] Reference [117], [b] Reference [118], [c] Reference [27], [d] Reference [58]

calculations.

C. Spin-orbit coupling parameters

Spin-orbit interaction, due to the relativistic coupling of electron angular motion and the electron spin, has already appeared in previous discussion of the g-tensor and zero-field-splitting. In this section we discuss first principles calculation of spin-orbit coupling parameters of point defect qubits in semiconductors that can be used to analyze the fine structure of the states and to investigate possible spin selective transitions between different defect states.

The spin-orbit interaction Hamiltonian in zero-order approximation can be written as[44]

$$\hat{H}_{\text{SO}} = \frac{1}{2}\frac{1}{c^2 m_e^2}\sum_i \left(\nabla_i V \times \hat{\mathbf{p}}_i\right)\hat{\mathbf{S}}_i, \tag{12}$$

where V is the nuclear potential energy, m_e is the electron mass, and $\hat{\mathbf{p}}_i$ and $\hat{\mathbf{S}}_i$ are the momentum and spin of electron i. The elements of the orbital operator vector $\hat{\mathbf{O}} = \nabla_i V \times \hat{\mathbf{p}}_i$ can be calculated from the Kohn-Sham orbitals. Note that the crystal field of a solid breaks the spherical symmetry of the spin-orbit interaction. In low symmetry case the interaction Hamiltonian can be rewritten as[44]

$$\hat{H}_{\text{SO}} = \sum_i \lambda_x \hat{L}_{i,x}\hat{S}_{i,x} + \lambda_y \hat{L}_{i,y}\hat{S}_{i,y} + \lambda_z \hat{L}_{i,z}\hat{S}_{i,z}, \tag{13}$$

where λ_a for $a \in \{x, y, z\}$ are the spin-orbit interaction parameters. In C_{3v} symmetry $\lambda_\perp = \lambda_x = \lambda_y$ and $\lambda_\parallel = \lambda_z$ are the basal or non-axial and axial parameters of the interaction, respectively. The former parameter is dominantly responsible for the mixing of different spin states, e.g. triplet and

singlet states, while axial parameter is mainly responsible for the splitting and shift of different spin-orbit coupled states. Note that the most frequently used $\lambda\hat{\mathbf{L}}\hat{\mathbf{S}}$ form is only recovered in higher symmetry cases when $\lambda = \lambda_\perp = \lambda_\parallel$. Note also that the above formula inherently includes the assumption that $\nabla_i V$ is identical for all the electronic states. This may be violated when systems of different atomic species are considered. In standard implementations available in first principles codes no such approximation is taken, however, the anisotropy of the spin-orbit interaction is generally neglected.[119–121]

In light element hosts, such as diamond and SiC, the spin-orbit coupling energy can be very small for localized point defect states, generally in the order of $10 - 100$ μeV (≈GHz). Furthermore, axial spin-orbit interaction is non-zero for states of non-zero effective spin and orbital momentum. Most often, the ground state of point defect qubits have no effective angular momentum, thus no axial spin-orbit contribution can be observed in the ground state ZFS.[44,46,47,55]

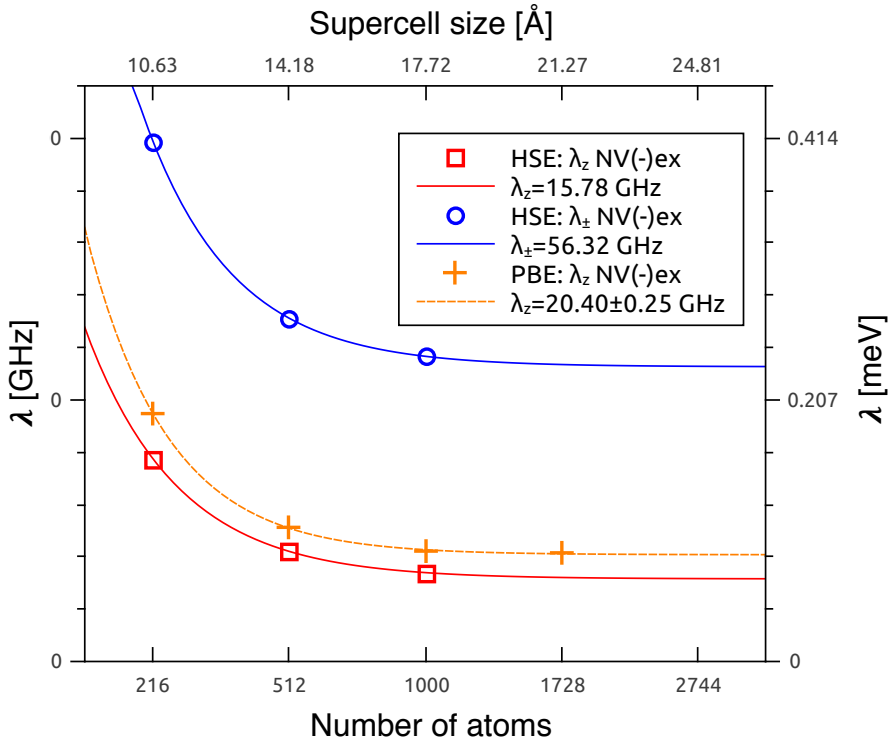

FIG. 4. Convergence of the axial spin-orbit coupling parameter λ in the excited state of NV center.[91] Horizontal axes shows the supercell size and the number of carbon atoms in the defect free supercells .

Spin-orbit interaction calculations for the NV center and for other potential qubits, group-IV-

vacancy color centers in diamond, have been pioneered by Thiering *et al.* in Refs. [91] and [122]. The axial spin-orbit interaction strength in the excited state can be obtained both from total energy difference calculations and from the splitting of Koghn-Sham states in constrained occupation non-collinear DFT calculations[91]. To accurately determine small values of the axial spin-orbit interaction, the calculations require high numerical convergence and accuracy. Finite size effect turned to be crucial for spin-orbit interaction calculations[91], see Fig. 4. Thiering *et al.* in Ref. [91] attributed the observed finite size effect to the overlap of the defect states and used an exponential fit to eliminate supercell size dependence of the λ_z. Note that axial spin-orbit coupling parameter calculations are only possible in the Γ-point of the Brillouin zone, as the dispersion and splitting of the defect states in low symmetry k-points may be larger than the axial spin-orbit splitting.

It is important to mention that due to the dynamic Jahn-Teller nature of the excited states of the considered defects, the calculated axial spin-orbit parameter cannot be directly compared with the experimental values[91]. The efficient electron-phonon coupling reduces the angular momentum of the electrons in the excited state. By taking into account this damping effect, the calculated axial spin-orbit parameters compare well with the experimental values[91,122]. On the other hand, the calculation of the non-axial component of the spin-orbit interaction requires further investigation and development.[91]

D. Hyperfine tensor calculation

The hyperfine interaction tensor describes the coupling of nuclear spin to the electron spin density of the point defect. As spin density is generally a unique feature of paramagnetic point defects, the hyperfine structure is an important fingerprint that can be utilized in point defect configuration identification. Indeed hyperfine interaction is probably the most frequently calculated spin dependent quantity of point defects in semiconductors.

Considering only linear term in spin operators, the hyperfine spin Hamiltonian of a single electron spin-nuclear spin pair can be written as

$$H_{\text{hyp}} = \hat{\mathbf{S}} A \hat{\mathbf{I}}, \tag{14}$$

where $\mathbf{A}$ is the hyperfine tensor and $\hat{\mathbf{I}}$ is the nuclear spin vector operator. When the electron spin density is non-zero at the place of the considered nuclear spin, the hyperfine tensor elements are

defined by the sum of two terms,

$$A_{ab} = \frac{2\mu_0}{3} g_e \mu_B g_N \mu_N \frac{\sigma(\mathbf{R})}{S} + \frac{\mu_0}{4\pi} g_e \mu_B g_N \mu_N \frac{1}{S} \int \frac{3r_a r_b - r^2 \delta_{ab}}{r^5} \sigma(\mathbf{r})\, d\mathbf{r}, \tag{15}$$

where $\sigma(\mathbf{r})$ is the electron spin density, $\mathbf{r}$ is the vector between the electron spin and nuclear spin at $\mathbf{R}$, g_N is the nuclear g-factor, and μ_N is the nuclear magneton. The first term on the right hand side of Eq. (15) is the Fermi contact term that describes isotropic magnetic interaction between the spins, while the second term on the right hand side of Eq. (15) is the anisotropic, long-ranged dipole-dipole interaction term. Note that in Eq. (15), we approximated the electron spin g-tensor with g_e.[104]

In case of an axial symmetric hyperfine interaction, i.e. when the nuclear spin is located on the symmetry axis of the systems, which becomes the quantization axis as well, the hyperfine tensor is diagonal with diagonal element $A_{xx} = A_{yy} = A_\perp$ and $A_{zz} = A_\parallel$. These parameters can be expressed by the Fermi-contact term a and a simplified dipolar coupling term b as $A_\perp = a - b$ and $A_\parallel = a + 2b$.

In the first implementation for DFT calculations with periodic boundary conditions by Van de Walle *et. al.* in Refs. [123] and [124], pseudopotentials were used and only the axial symmetric hyperfine interaction parameters were calculated. This approach was successfully applied in the identification of electron paramagnetic resonance (EPR) centers in semiconductors, see for example the citations of Ref. [124]. Later, the theory was extended to Greens' function[125] calculations and PAW full hyperfine tensor calculations[70,126]. According to recent numerical tests, HSE06 hybrid functional hyperfine calculations including core polarization correction[70,127,128] provides the most accurate results[70].

Hyperfine interaction calculations have been carried out for the most important point defect qubits, such as the NV center[70,129], divacancy[27], and silicon vacancy[43,70]. Recently, hyperfine tensors were calculated not only for the first and second neighbor nuclei sites, but also for more distant nuclei sites that are usually not resolvable in experiments.[43,130]

Similarly to the case of electron spin-electron spin dipolar interaction, finite size effects are expected in the hyperfine values that are calculated with periodic boundary conditions. Indeed, using the implementation provided in Ref. [70], considerable finite size effects where reported in Ref. [42], see Fig. 5. As can be seen, the relative error increases for nuclei sites located farther away from a divacancy point defect qubit. Importantly, both the Fermi contact and the dipole-dipole interaction terms exhibit finite size effects, which however rapidly reduce with increasing

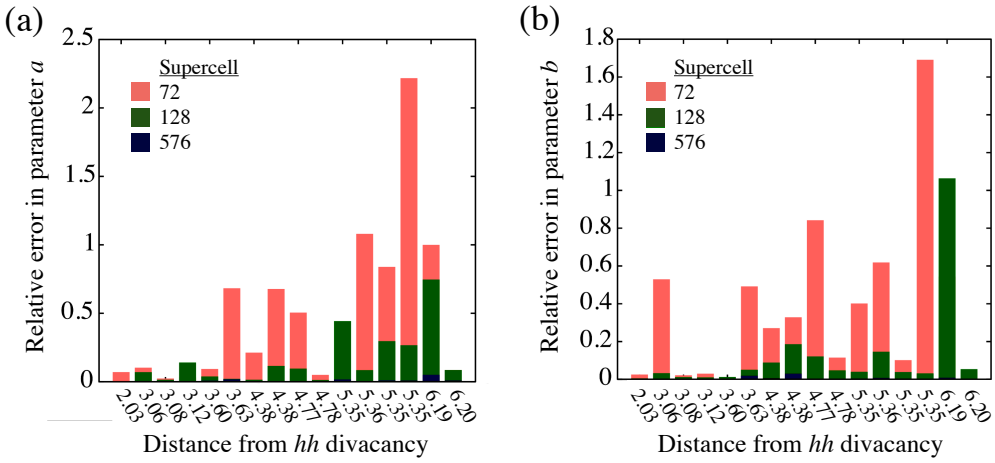

FIG. 5. Relative error of the calculated (a) Fermi contact and (b) dipole-dipole hyperfine interaction strength for various nuclei sites around a hh divacancy in 4H SiC.[42] On the horizontal axis the distances from the silicon vacancy site of the divacancy are given. Calculations are carried out in 72, 128, and 576 atom supercell using PBE functional. Deviations in the hyperfine values are measured from the parameters obtained in the absolutely convergent 2400 atom supercell.

supercell size. These observations suggest that the overlap of the defects states is responsible for the reported finite size effects. Consequently, accurate calculation of hyperfine tensor of distant nuclei sites is only possible in large supercells, where the overlap of the defect states is negligible. Finally, we would like to mention that the finite size effect caused by the long-ranged dipole-dipole interaction term can be easily eliminated by employing real space integration instead of the commonly applied momentum space integration.

The simulations of shallow donor qubits in silicon quantum dots are especially challenging[131] due to the delocalization of the defect states and the substantial finite size effects. To overcome some of these problems and, at the same time, to investigate the quantum confinement effects, cluster models are frequently used in hyperfine parameter calcaultions of these qubits.[132,133]

E. Other coupling parameters

In the previous sections we discussed first principles calculations of the most important spin related quantities of point defect qubits. At the same time, there are numerous further coupling terms and coupling parameters that can be derived from relativistic perturbation theory.[134] Restricting ourselves to terms of $\mathcal{O}(\alpha^0)$ and $\mathcal{O}(\alpha^2)$, where $\alpha \approx 1/137$ is the fine-structure constant, the

following spin and orbital momentum related interaction terms can appear: i) nuclear quadrupole interaction ($\mathcal{O}(\alpha^0)$), ii) electron orbital-orbital dipole interaction, iii) spin-spin contact interaction, iv) orbital hyperfine interaction, and v) magnetic field dependent corrections terms to the spin-orbit, spin-other-orbit, nuclear Zeeman, and orbital-hyperfine interactions. There are available implementations for the nuclear quadruple[135,136] and orbital hyperfine interaction terms[137–139]. However, to the best of our knowledge these terms have not been considered in the context of first principles point defect qubit calculations. Investigation of higher order terms may be important for highly accurate first principles calculations and for studying exotic spin state couplings.

F. Role of electron-phonon coupling

Although, electron-phonon coupling is not a spin dependent phenomena, it still can indirectly affect the expectation values of spin dependent observables, as we have already seen in the case of spin-orbit interaction in section IV C. In general, when the adiabatic approximation is violated, mixed electronic and vibronic wavefunctions are required to accurately calculate orbital dependent spin coupling parameters such as g-tensor, zero-field-splitting, and spin-orbit interaction parameters. Therefore, here we shortly review relevant works on the description of electron-phonon coupling in point defect qubits.

Ground or excited states of point defects often exhibit different Jahn-Teller instabilities. In the dynamic Jahn-Teller effect, when the zero-point motion or thermally occupied phonon modes have sufficient energy to continuously drive the system between different Jahn-Teller distorted states, the electron states and phonon modes strongly couple. Recently, model Hamiltonian approach was applied to investigate the triplet excited state of the NV center in diamond, which is a dynamic Jahn-Teller system, where the partially occupied e single particle state couples to a localized E vibrational mode. Abtew *et al.* in Ref. [140] and Thiering *et al.* in Ref. [91] applied a so called $e \otimes E$ model, in which a model potential energy surface of the e electronic states over generalized coordinate space of the E vibrational mode is parameterized by constrained occupation DFT calculations. The electron-phonon coupling potential established this way is added to the Hamiltonian of the $e \otimes E$ model system and solved by exact diagonalization. Even in the vibrational ground state, different electronic states of different angular momentum are mixed with vibronic states. As a consequence, the $L = 2$ angular momentum of the excited state electronic configuration is quenched down by 70% in the vibronic ground state, resulting in theoretical axial spin-orbit

coupling parameter compares well with the experiment.[91] Note that similar theory should be applied to the g-tensor calculation in the excited state. The zero-field-splitting of the vibronic ground state has not been investigated yet.

V. SUMMARY AND OUTLOOK

Point defect quantum bits in semiconductors are among the most recent inventions of solid-state physicists and material scientists that may serve as building units for room temperature controlled quantum systems in semiconductors. Additionally, point defect quantum bits provide an interface for investigating materials and molecules with nanoscale spatial resolution. As these elementary solid state quantum devices can be directly and quantitatively studied by first principles calculations, theoretical studies hold a great promise for fast development of these areas.

As we have shown here, methodology and implementations for the calculations of the most important ground state spin dependent quantities have already been demonstrated in the literature. In general, applications of these methods show considerable accuracy and predictive power, which is encouraging for broadening the range of simulations. On the other hand, there is a great need in further developments. In some cases, the limitations of the currently used method or technical requirements of completely convergent calculations are still unknown. Furthermore, higher order coupling term calculations might be considered in the future.

Calculations of excited state spin dependent properties, however, still remain quite challenging. The reason to this is twofold. First, proper excited state electronic structure calculations require to go beyond conventional applications of the DFT. Second, the electron-phonon coupling tends to play an important role in some properties of the excited states. Calculation of the spin dependent quantities will become significantly more reliable upon overcoming the above mentioned methodological challenges.

A. Future applications

Finally, we would like to call attention to two possible future applications for the existing and required first principles methods mentioned in this Highlight.

1. First principles predictions of point defect qubits

There are numerous two and three dimensional semiconducting materials that have been synthesized so far and their number is increasing day by day. Many of these materials can host paramagnetic point defects that may exhibit potential for implementing novel point defect qubits. Using first principles calculations is the most suitable approach for fast investigation of this vast

unexplored field. Requirements for systematic point defect search have been discussed in the literature[42]. Moreover, it has been shown that computationally efficient methods can be used for high throughput screening of point defect by calculating the defects spin states and basic optical properties[42,141]. The evaluation of candidate paramagnetic point defects real potential for qubit applications, however, requires more detailed studies by using methods summarized in this paper. For such systematic point defect qubit search, appropriate highly automated search algorithms are yet to be developed.

2. Ab initio *support for predictive spin dynamic simulations*

Simulations in the framework of model spin Hamiltonian for qualitative understanding of basic functionalities of point defect qubits is an other emerging direction for theoretical studies. These simulations generally relay on spin coupling and other system specific parameters that at present are usually obtained from experimental measurements. Accurate measurement of all of the required parameters is cumbersome and not always possible, thus spin Hamiltonian models frequently contain free parameters as well. Consequently, quantitative predictive power and transferability of these methods are highly limited.

On the other hand, first principles calculations of spin related parameters of point defect qubits may take over the role of experimental measurements. Combining *ab initio* calculations with model spin Hamiltonian approaches may results in novel methodologies that allow for parameter free quantitatively predictive spin dynamic simulations. Such method would be highly important not only for quantitative understanding of the physics of point defect spins but also for modeling the operation and applications of point defect qubit candidates.

Indeed, in recent spin dynamic simulations for optical dynamic nuclear polarization (ODNP) thorough divacancy quantum bits, *ab initio* hyperfine tensors were used in the simulations that allowed the prediction of fine structures in the magnetic field dependence of the nuclear spin polarization, which were confirmed in experiment.[142] This example demonstrates the potential of *ab intio* theory supported spin Hamiltonian approaches.

ACKNOWLEDGMENTS

Discussions with Gergő Thiering and Zoltán Bodrog are highly appreciated. Support from the Swedish Government Strategic Research Areas in Materials Science on Functional Materials at Linkping University (Faculty Grant SFO-Mat-LiU No. 2009-00971) and Knut & Alice Wallenberg Foundation New States of Matter 2014-2019 (COTXS) is gratefully acknowledged. Analysis of first-principles calculations of defect properties was supported by the Ministry of Education and Science of the Russian Federation (Grant No. 14.Y26.31.0005). Applications of the model Hamiltonians were supported by the Ministry of Education and Science of the Russian Federation in the framework of Increase Competitiveness Program of NUST MISIS (No K2-2017-080) implemented by a governmental decree dated 16 March 2013, No 211. AG acknowledges the support from the National Research Development and Innovation Office of Hungary within the Quantum Technology National Excellence Program (Project No. 2017-1.2.1-NKP-2017-00001).

---

[1] T. D. Ladd, F. Jelezko, R. Laflamme, Y. Nakamura, C. Monroe, and J. L. O'Brien, Nature **464**, 45 (2010).

[2] J. Wrachtrup and F. Jelezko, Journal of Physics-Condensed Matter **18**, S807 (2006).

[3] J. R. Weber, W. F. Koehl, J. B. Varley, A. Janotti, B. B. Buckley, C. G. Van de Walle, and D. D. Awschalom, PNAS **107**, 8513 (2010).

[4] M. V. G. Dutt, L. Childress, L. Jiang, E. Togan, J. Maze, F. Jelezko, A. S. Zibrov, P. R. Hemmer, and M. D. Lukin, Science **316**, 1312 (2007).

[5] B. E. Kane, Nature **393**, 133 (1998).

[6] R. Vrijen, E. Yablonovitch, K. Wang, H. W. Jiang, A. Balandin, V. Roychowdhury, T. Mor, and D. DiVincenzo, Phys. Rev. A **62**, 012306 (2000).

[7] D. D. Awschalom, L. C. Bassett, A. S. Dzurak, E. L. Hu, and J. R. Petta, Science **339**, 1174 (2013).

[8] A. M. Tyryshkin, S. Tojo, J. J. L. Morton, H. Riemann, N. V. Abrosimov, P. Becker, H.-J. Pohl, T. Schenkel, M. L. W. Thewalt, K. M. Itoh, and S. A. Lyon, Nature Materials **11**, 143 EP (2011).

[9] G. Balasubramanian, P. Neumann, D. Twitchen, M. Markham, R. Kolesov, N. Mizuochi, J. Isoya, J. Achard, J. Beck, J. Tissler, V. Jacques, P. R. Hemmer, F. Jelezko, and J. Wrachtrup, Nature Mater. **8**, 383 (2009).

[10] W. F. Koehl, B. B. Buckley, F. J. Heremans, G. Calusine, and D. D. Awschalom, Nature **479**, 84 (2011).

[11] M. Widmann, S.-Y. Lee, T. Rendler, N. T. Son, H. Fedder, S. Paik, L.-P. Yang, N. Zhao, S. Yang, I. Booker, A. Denisenko, M. Jamali, S. A. Momenzadeh, I. Gerhardt, T. Ohshima, A. Gali, E. Janzén, and J. Wrachtrup, Nat Mater **14**, 164 (2015).

[12] G. Kucsko, P. C. Maurer, N. Y. Yao, M. Kubo, H. J. Noh, P. K. Lo, H. Park, and M. D. Lukin, Nature **500**, 54 EP (2013).

[13] T. Iwasaki, W. Naruki, K. Tahara, T. Makino, H. Kato, M. Ogura, D. Takeuchi, S. Yamasaki, and M. Hatano, ACS Nano **11**, 1238 (2017), pMID: 28112891, https://doi.org/10.1021/acsnano.6b04460.

[14] M. S. J. Barson, P. Peddibhotla, P. Ovartchaiyapong, K. Ganesan, R. L. Taylor, M. Gebert, Z. Mielens, B. Koslowski, D. A. Simpson, L. P. McGuinness, J. McCallum, S. Prawer, S. Onoda, T. Ohshima, A. C. Bleszynski Jayich, F. Jelezko, N. B. Manson, and M. W. Doherty, Nano Letters **17**, 1496 (2017), pMID: 28146361, https://doi.org/10.1021/acs.nanolett.6b04544.

[15] G. Balasubramanian, I. Y. Chan, R. Kolesov, M. Al-Hmoud, J. Tisler, C. Shin, C. Kim, A. Wojcik, P. R. Hemmer, A. Krueger, T. Hanke, A. Leitenstorfer, R. Bratschitsch, F. Jelezko, and J. Wrachtrup, Nature **455**, 648 (2008).

[16] H. J. Mamin, M. Kim, M. H. Sherwood, C. T. Rettner, K. Ohno, D. D. Awschalom, and D. Rugar, Science **339**, 557 (2013), http://science.sciencemag.org/content/339/6119/557.full.pdf.

[17] N. Aslam, M. Pfender, P. Neumann, R. Reuter, A. Zappe, F. Fávaro de Oliveira, A. Denisenko, H. Sumiya, S. Onoda, J. Isoya, and J. Wrachtrup, Science **357**, 67 (2017), http://science.sciencemag.org/content/357/6346/67.full.pdf.

[18] T. Wolf, P. Neumann, K. Nakamura, H. Sumiya, T. Ohshima, J. Isoya, and J. Wrachtrup, Phys. Rev. X **5**, 041001 (2015).

[19] S.-Y. Lee, M. Niethammer, and J. Wrachtrup, Phys. Rev. B **92**, 115201 (2015).

[20] M. Ledbetter, K. Jensen, R. Fischer, A. Jarmola, and D. Budker, Phys. Rev. A **86**, 052116 (2012).

[21] A. Ajoy and P. Cappellaro, Phys. Rev. A **86**, 062104 (2012).

[22] L. Childress, J. M. Taylor, A. S. Sørensen, and M. D. Lukin, Phys. Rev. Lett. **96**, 070504 (2006).

[23] H. Bernien, B. Hensen, W. Pfaff, G. Koolstra, M. S. Blok, L. Robledo, T. H. Taminiau, M. Markham, D. J. Twitchen, L. Childress, and R. Hanson, Nature **497**, 86 EP (2013).

[24] B. Hensen, H. Bernien, A. E. Dréau, A. Reiserer, N. Kalb, M. S. Blok, J. Ruitenberg, R. F. L. Vermeulen, R. N. Schouten, C. Abellán, W. Amaya, V. Pruneri, M. W. Mitchell, M. Markham, D. J. Twitchen, D. Elkouss, S. Wehner, T. H. Taminiau, and R. Hanson, Nature **526**, 682 EP (2015).

[25] G. Tosi, F. A. Mohiyaddin, V. Schmitt, S. Tenberg, R. Rahman, G. Klimeck, and A. Morello, Nature Communications **8**, 450 (2017).

[26] V. Jacques, P. Neumann, J. Beck, M. Markham, D. Twitchen, J. Meijer, F. Kaiser, G. Balasubramanian, F. Jelezko, and J. Wrachtrup, Phys. Rev. Lett. **102**, 057403 (2009).

[27] A. L. Falk, P. V. Klimov, V. Ivády, K. Szász, D. J. Christle, W. F. Koehl, A. Gali, and D. D. Awschalom, Phys. Rev. Lett. **114**, 247603 (2015).

[28] J. P. King, K. Jeong, C. C. Vassiliou, C. S. Shin, R. H. Page, C. E. Avalos, H.-J. Wang, and A. Pines, Nat Commun **6** (2015).

[29] A. M. Tyryshkin, S. A. Lyon, A. V. Astashkin, and A. M. Raitsimring, Phys. Rev. B **68**, 193207 (2003).

[30] M. H. Mohammady, G. W. Morley, and T. S. Monteiro, Phys. Rev. Lett. **105**, 067602 (2010).

[31] P. V. Klimov, A. L. Falk, D. J. Christle, V. V. Dobrovitski, and D. D. Awschalom, Science Advances **1** (2015), 10.1126/sciadv.1501015, http://advances.sciencemag.org/content/1/10/e1501015.full.pdf.

[32] I. Aharonovich, S. Castelletto, D. A. Simpson, A. Stacey, J. McCallum, A. D. Greentree, and P. S., Nano Letters **9**, 3191 (2009).

[33] S. Castelletto, B. C. Johnson, V. Ivády, N. Stavrias, T. Umeda, A. Gali, and T. Ohshima, Nat. Mater. **13**, 151 (2014).

[34] R. Kolesov, K. Xia, R. Reuter, R. Stöhr, A. Zappe, J. Meijer, P. R. Hemmer, and J. Wrachtrup, Nature Communications **3**, 1029 (2012).

[35] J. R. Maze, P. L. Stanwix, J. S. Hodges, S. Hong, J. M. Taylor, P. Cappellaro, L. Jiang, M. V. G. Dutt, E. Togan, A. S. Zibrov, A. Yacoby, R. L. Walsworth, and M. D. Lukin, Nature **455**, 644 (2008).

[36] B. B. Buckley, G. D. Fuchs, L. C. Bassett, and D. D. Awschalom, Science **330**, 1212 (2010).

[37] L. Robledo, L. Childress, H. Bernien, B. Hensen, P. F. A. Alkemade, and R. Hanson, Nature **477**, 574 (2011).

[38] D. J. Christle, A. L. Falk, P. Andrich, P. V. Klimov, J. U. Hassan, N. T. Son, E. Janzén, T. Ohshima, and D. D. Awschalom, Nat Mater **14**, 160 (2015).

[39] V. A. Soltamov, A. A. Soltamova, P. G. Baranov, and I. I. Proskuryakov, Phys. Rev. Lett. **108**, 226402 (2012).

[40] A. L. Falk, B. B. Buckley, G. Calusine, W. F. Koehl, V. V. Dobrovitski, A. Politi, C. A. Zorman, P. X.-L. Feng, and D. D. Awschalom, Nature Commun. **4**, 1819 (2013).

[41] L. Gordon, A. Janotti, and C. G. Van de Walle, Phys. Rev. B **92**, 045208 (2015).

[42] J. Davidsson, V. Ivdy, R. Armiento, N. T. Son, A. Gali, and I. A. Abrikosov, New Journal of Physics **20**, 023035 (2018).

[43] V. Ivády, J. Davidsson, N. T. Son, T. Ohshima, I. A. Abrikosov, and A. Gali, Phys. Rev. B **96**, 161114 (2017).

[44] J. R. Maze, A. Gali, E. Togan, Y. Chu, A. Trifonov, E. Kaxiras, and M. D. Lukin, New Journal of Physics **13**, 025025 (2011).

[45] M. W. Doherty, N. B. Manson, P. Delaney, and L. C. L. Hollenberg, New Journal of Physics **13**, 025019 (2011).

[46] O. O. Soykal, P. Dev, and S. E. Economou, Phys. Rev. B **93**, 081207 (2016).

[47] A. Gali, A. Gällström, N. Son, and E. Janzén, Mater. Sci. Forum **645-648**, 395 (2010).

[48] A. Gali, M. Fyta, and E. Kaxiras, Phys. Rev. B **77**, 155206 (2008).

[49] J. H. N. Loubser and J. A. van Wyk, Reports on Progress in Physics **41**, 1201 (1978).

[50] N. Son, P. Carlsson, J. ul Hassan, E. Janzén, T. Umeda, J. Isoya, A. Gali, M. Bockstedte, N. Morishita, T. Ohshima, and H. Itoh, Phys. Rev. Lett. **96**, 055501 (2006).

[51] P. Tamarat, N. B. Manson, J. P. Harrison, R. L. McMurtrie, A. Nizovtsev, C. Santori, R. G. Beausoleil, P. Neumann, T. Gaebel, F. Jelezko, and J. Hemmer, P. Wrachtrup, New Journal of Physics **10**, 045004 (2008).

[52] A. Batalov, V. Jacques, F. Kaiser, P. Siyushev, P. Neumann, L. J. Rogers, R. L. McMurtrie, N. B. Manson, F. Jelezko, and J. Wrachtrup, Phys. Rev. Lett. **102**, 195506 (2009).

[53] D. J. Christle, P. V. Klimov, C. F. de las Casas, K. Szász, V. Ivády, V. Jokubavicius, J. Ul Hassan, M. Syväjärvi, W. F. Koehl, T. Ohshima, N. T. Son, E. Janzén, A. Gali, and D. D. Awschalom, Phys. Rev. X **7**, 021046 (2017).

[54] L. J. Rogers, R. McMurtrie, M. Sellars, and N. B. Manson, New Journal of Physics **11**, 063007 (2009).

[55] M. W. Doherty, N. B. Manson, P. Delaney, F. Jelezko, J. Wrachtrup, and L. C. Hollenberg, Physics Reports **528**, 1 (2013), the nitrogen-vacancy colour centre in diamond.

[56] F. Jelezko, T. Gaebel, I. Popa, A. Gruber, and J. Wrachtrup, Physical Review Letters **92**, 076401 (2004).

[57] A. Gali, J. Mat. Res. **27**, 897 (2012).

[58] A. N. Anisimov, D. Simin, V. A. Soltamov, S. P. Lebedev, P. G. Baranov, G. V. Astakhov, and V. Dyakonov, Scientific Reports **6**, 33301 (2016).

[59] F. Jelezko, T. Gaebel, I. Popa, M. Domhan, A. Gruber, and J. Wrachtrup, Phys. Rev. Lett. **93**, 130501 (2004).

[60] P. Hohenberg and W. Kohn, Phys. Rev. **136**, B864 (1964).

[61] R. O. Jones, Rev. Mod. Phys. **87**, 897 (2015).

[62] W. Kohn and L. J. Sham, Phys. Rev. **140**, A1133 (1965).

[63] W. Kohn, Rev. Mod. Phys. **71**, 1253 (1999).

[64] A. Seidl, A. Görling, P. Vogl, J. A. Majewski, and M. Levy, Phys. Rev. B **53**, 3764 (1996).

[65] J. P. Perdew, K. Burke, and M. Ernzerhof, Phys. Rev. Lett. **77**, 3865 (1996).

[66] J. Heyd, G. E. Scuseria, and M. Ernzerhof, J. Chem. Phys. **118**, 8207 (2003).

[67] J. Heyd, G. E. Scuseria, and M. Ernzerhof, J. Chem. Phys. **124**, 219906 (2006).

[68] T. M. Henderson, J. Paier, and G. E. Scuseria, physica status solidi (b) **248**, 767 (2010).

[69] P. Deák, B. Aradi, T. Frauenheim, E. Janzén, and A. Gali, Phys. Rev. B **81**, 153203 (2010).

[70] K. Szász, T. Hornos, M. Marsman, and A. Gali, Phys. Rev. B **88**, 075202 (2013).

[71] J. P. Perdew, R. G. Parr, M. Levy, and J. L. Balduz, Phys. Rev. Lett. **49**, 1691 (1982).

[72] F. Iori, M. Gatti, and A. Rubio, Phys. Rev. B **85**, 115129 (2012).

[73] P. Deák, Q. Duy Ho, F. Seemann, B. Aradi, M. Lorke, and T. Frauenheim, Phys. Rev. B **95**, 075208 (2017).

[74] J. P. Perdew and A. Zunger, Phys. Rev. B **23**, 5048 (1981).

[75] V. Ivády, I. A. Abrikosov, E. Janzén, and A. Gali, Phys. Rev. B **87**, 205201 (2013).

[76] V. Ivády, R. Armiento, K. Szász, E. Janzén, A. Gali, and I. A. Abrikosov, Phys. Rev. B **90**, 035146 (2014).

[77] P. E. Blöchl, Phys. Rev. B **50**, 17953 (1994).

[78] A. Beste and D. E. Taylor, *Convergence of Ground and Excited State Properties of Divacancy Defects in 4H-SiC with Computational Cell Size*, Tech. Rep. ARL-TR-8313 (2018).

[79] A. Gali, E. Janzén, P. Deák, G. Kresse, and E. Kaxiras, Phys. Rev. Lett. **103**, 186404 (2009).

[80] C. E. Dreyer, A. Alkauskas, J. L. Lyons, A. Janotti, and C. G. V. de Walle, Annual Review of Materials Research **48**, null (2018), https://doi.org/10.1146/annurev-matsci-070317-124453.

[81] G. Davies and M. F. Hamer, Proceedings of the Royal Society of London. Series A **348**, 285 (1976).

[82] S. Lany and A. Zunger, Phys. Rev. B **80**, 085202 (2009).

[83] I. Dabo, A. Ferretti, N. Poilvert, Y. Li, N. Marzari, and M. Cococcioni, Phys. Rev. B **82**, 115121 (2010).

[84] J. P. Perdew and M. Levy, Phys. Rev. B **56**, 16021 (1997).

[85] H.-P. Komsa, T. T. Rantala, and A. Pasquarello, Phys. Rev. B **86**, 045112 (2012).

[86] Y. Ma, M. Rohlfing, and A. Gali, Phys. Rev. B **81**, 041204 (2010).

[87] P. Delaney, J. C. Greer, and J. A. Larsson, Nano Letters **10**, 610 (2010), pMID: 20085271, http://pubs.acs.org/doi/pdf/10.1021/nl903646p.

[88] A. Ranjbar, M. Babamoradi, M. Heidari Saani, M. A. Vesaghi, K. Esfarjani, and Y. Kawazoe, Phys. Rev. B **84**, 165212 (2011).

[89] S. Choi, M. Jain, and S. G. Louie, Phys. Rev. B **86**, 041202 (2012).

[90] L. J. Rogers, S. Armstrong, M. J. Sellars, and N. B. Manson, New Journal of Physics **10**, 103024 (2008).

[91] G. Thiering and A. Gali, Phys. Rev. B **96**, 081115 (2017).

[92] L. Hedin, Phys. Rev. **139**, A796 (1965).

[93] E. E. Salpeter and H. A. Bethe, Phys. Rev. **84**, 1232 (1951).

[94] P. J. Stephens, F. J. Devlin, C. F. Chabalowski, and M. J. Frisch, The Journal of Physical Chemistry **98**, 11623 (1994), https://doi.org/10.1021/j100096a001.

[95] G. Schreckenbach and T. Ziegler, The Journal of Physical Chemistry A **101**, 3388 (1997), https://doi.org/10.1021/jp963060t.

[96] J. E. Harriman, *Theoretical foundations of electron spin resonance* (Academic Press, 1978).

[97] C. J. Pickard and F. Mauri, Phys. Rev. Lett. **88**, 086403 (2002).

[98] D. Sebastiani and M. Parrinello, The Journal of Physical Chemistry A **105**, 1951 (2001), https://doi.org/10.1021/jp002807j.

[99] R. Declerck, V. Van Speybroeck, and M. Waroquier, Phys. Rev. B **73**, 115113 (2006).

[100] C. J. Pickard and F. Mauri, Phys. Rev. B **63**, 245101 (2001).

[101] E. S. Kadantsev and T. Ziegler, The Journal of Physical Chemistry A **113**, 1327 (2009), pMID: 19173640, https://doi.org/10.1021/jp805466c.

[102] H. J. von Bardeleben, J. L. Cantin, E. Rauls, and U. Gerstmann, Phys. Rev. B **92**, 064104 (2015).

[103] H. J. von Bardeleben, J. L. Cantin, A. Csóré, A. Gali, E. Rauls, and U. Gerstmann, Phys. Rev. B **94**, 121202 (2016).

[104] J. A. Weil and J. R. Bolton, *Electron Paramagnetic Resonance: Elementary Theory and Practical Applications* (John Wiley & Sons, 2007).

[105] D. G. McGavin and W. C. Tennant, Journal of Physics: Condensed Matter **21**, 245501 (2009).

[106] D. Simin, V. A. Soltamov, A. V. Poshakinskiy, A. N. Anisimov, R. A. Babunts, D. O. Tolmachev, E. N. Mokhov, M. Trupke, S. A. Tarasenko, A. Sperlich, P. G. Baranov, V. Dyakonov, and G. V. Astakhov, Phys. Rev. X **6**, 031014 (2016).

[107] M. Kaupp, M. Bhl, and V. G. Malkin, *Calculation of NMR and EPR Parameters: Theory and Applications* (John Wiley & Sons, 2004).

[108] M. J. Rayson and P. R. Briddon, Phys. Rev. B **77**, 035119 (2008).

[109] M. Rayson, J. Goss, and P. Briddon, Physica B: Condensed Matter **340-342**, 673 (2003), proceedings of the 22nd International Conference on Defects in Semiconductors.

[110] V. Ivády, T. Simon, J. R. Maze, I. A. Abrikosov, and A. Gali, Phys. Rev. B **90**, 235205 (2014).

[111] H. Seo, H. Ma, M. Govoni, and G. Galli, Phys. Rev. Materials **1**, 075002 (2017).

[112] Z. Bodrog and A. Gali, Journal of Physics: Condensed Matter **26**, 015305 (2014).

[113] T. Biktagirov, W. G. Schmidt, and U. Gerstmann, Phys. Rev. B **97**, 115135 (2018).

[114] A. L. Falk, P. V. Klimov, B. B. Buckley, V. Ivády, I. A. Abrikosov, G. Calusine, W. F. Koehl, A. Gali, and D. D. Awschalom, Phys. Rev. Lett. **112**, 187601 (2014).

[115] M. Wagner, B. Magnusson, W. M. Chen, E. Janzén, E. Sörman, C. Hallin, and J. L. Lindström, Phys. Rev. B **62**, 16555 (2000).

[116] P. Udvarhelyi, V. O. Shkolnikov, A. Gali, G. Burkard, and A. Plyi, e-print arXiv: **1712.02684** (2017).

[117] V. Ivády, I. A. Abrikosov, and A. Gali, unpublished data.

[118] G. Fuchs, V. Dobrovitski, R. Hanson, A. Batra, C. Weis, T. Schenkel, and D. Awschalom, Phys. Rev. Lett. **101**, 117601 (2008).

[119] X. Gonze, J.-M. Beuken, R. Caracas, F. Detraux, M. Fuchs, G.-M. Rignanese, L. Sindic, M. Verstraete, G. Zerah, F. Jollet, M. Torrent, A. Roy, M. Mikami, P. Ghosez, J.-Y. Raty, and D. Allan, Computational Materials Science **25**, 478 (2002).

[120] A. D. Corso and A. M. Conte, Phys. Rev. B **71**, 115106 (2005).

[121] S. Steiner, S. Khmelevskyi, M. Marsmann, and G. Kresse, Phys. Rev. B **93**, 224425 (2016).

[122] G. Thiering and A. Gali, Phys. Rev. X **8**, 021063 (2018).

[123] C. G. Van de Walle, Phys. Rev. Lett. **64**, 669 (1990).

[124] C. G. Van de Walle and P. E. Blöchl, Phys. Rev. B **47**, 4244 (1993).

[125] U. Gerstmann, physica status solidi (b) **248**, 1319 (2010), https://onlinelibrary.wiley.com/doi/pdf/10.1002/pssb.201046237.

[126] P. E. Blöchl, Phys. Rev. B **62**, 6158 (2000).

[127] O. V. Yazyev, I. Tavernelli, L. Helm, and U. Röthlisberger, Phys. Rev. B **71**, 115110 (2005).

[128] M. S. Bahramy, M. H. F. Sluiter, and Y. Kawazoe, Phys. Rev. B **76**, 035124 (2007).

[129] A. Gali, Phys. Rev. B **80**, 241204 (2009).

[130] V. Ivády, K. Szász, A. L. Falk, P. V. Klimov, D. J. Christle, E. Janzén, I. A. Abrikosov, D. D. Awschalom, and A. Gali, Phys. Rev. B **92**, 115206 (2015).

[131] J. S. Smith, A. Budi, M. C. Per, N. Vogt, D. W. Drumm, L. C. L. Hollenberg, J. H. Cole, and S. P. Russo, Scientific Reports **7**, 6010 (2017).

[132] D. V. Melnikov and J. R. Chelikowsky, Phys. Rev. Lett. **92**, 046802 (2004).

[133] B. Yan, R. Rurali, and Á. Gali, *Nano Letters*, Nano Letters **12**, 3460 (2012).

[134] P. Manninen, *Breit-Pauli Hamiltonian and Molecular Magnetic Resonance Properties*, Ph.D. thesis, University of Oulu (2004).

[135] H. M. Petrilli, P. E. Blöchl, P. Blaha, and K. Schwarz, Phys. Rev. B **57**, 14690 (1998).

[136] T. Charpentier, Solid State Nuclear Magnetic Resonance **40**, 1 (2011).

[137] S. Blügel, H. Akai, R. Zeller, and P. H. Dederichs, Phys. Rev. B **35**, 3271 (1987).

[138] P. Novák, *Calculation of hyperfine field in WIEN2k*, Tech. Rep. (2005).

[139] V. Chlan, H. tpnkov, R. eznek, and P. Novk, Solid State Nuclear Magnetic Resonance **40**, 27 (2011).

[140] T. A. Abtew, Y. Y. Sun, B.-C. Shih, P. Dev, S. B. Zhang, and P. Zhang, Phys. Rev. Lett. **107**, 146403 (2011).

[141] B. Lucatto, L. V. C. Assali, R. R. Pela, M. Marques, and L. K. Teles, Phys. Rev. B **96**, 075145 (2017).

[142] V. Ivády, P. V. Klimov, K. C. Miao, A. L. Falk, D. J. Christle, K. Szász, I. A. Abrikosov, D. D. Awschalom, and A. Gali, Phys. Rev. Lett. **117**, 220503 (2016).